VARIATIONAL AUTOENCODERS FOR HIGHLY MULTIVARIATE SPATIAL POINT PROCESSES INTENSITIES

Anonymous authors
Paper under double-blind review

ABSTRACT

Multivariate spatial point process models can describe heterotopic data over space. However, highly multivariate intensities are computationally challenging due to the curse of dimensionality. To bridge this gap, we introduce a declustering based hidden variable model that leads to an efficient inference procedure via a variational autoencoder (VAE). We also prove that this model is a generalization of the VAE-based model for collaborative filtering. This leads to an interesting application of spatial point process models to recommender systems. Experimental results show the method's utility on both synthetic data and real-world data sets.

1 INTRODUCTION

Multivariate point processes are widely used to model events of multiple types occurring in an n dimensional continuum. This paper focuses on multivariate spatial point processes, which can uncover hidden connections between subprocesses based on the correlations of their spatial point patterns. Often we encounter missing data problems, where some subprocesses are not fully observable. The underlying connections could further contribute to the prediction of these subprocesses over the unobserved areas. Moreno-Muñoz et al. (2018) has shown the effectiveness of this joint model for Gaussian processes with heterotopic data. Multi-output models in Lian et al. (2015) such as coregionalization and cokriging can outperform independent predictions. However, there is limited literature on the statistical methodology of the highly multivariate spatial point processes, according to the very recent paper (Choiruddin et al., 2019).

Inference for multivariate spatial point processes intensities is still a challenging problem (Taylor et al., 2015), especially with a large number of subprocesses. For popular Gaussian processes-based approaches (Williams & Rasmussen, 2006), the multivariate intensity often consists of independent and multi-output Gaussian processes. The complexity of the models and the curse of dimensionality hinder this approach for highly multivariate data, such as friendship networks and recommender systems with millions of users. In these problems, we only partially observe the events (e.g. users interact with items, locations) for each subprocess (user). It is necessary to jointly infer the preference of each user based on their hidden correlations. For example, a common approach in recommender systems, collaborative filtering (He et al., 2017), predicts the item interests of each user with the help of the collection of item preferences for a large number of users.

To address these problems, we propose a multivariate spatial point process model with a nonparametric intensity. We extend the well-known kernel estimator in Diggle (1985) to the multivariate case. This generalization is achieved through the introduction of hidden variables inspired by stochastic declustering (Zhuang et al., 2002). The latent variables naturally lead to a variational Bayesian inference approach, which is different from the frequentist point estimation in the kernel estimator. To reduce the complexity in the highly multivariate case, we consider an alternative set of hidden variables that are designed to work well as latent variables for a variational autoencoder (VAE) (Kingma & Welling, 2014). This amortized inference (Gershman & Goodman, 2014) approach leads to fast inference once the model is fully trained. Further, we show the equivalence for these two different settings of hidden variables using the properties of the spatial point process. This efficient approach makes it possible to apply multivariate spatial point processes in many areas, including recommender systems with a large number of users. Moreover, the nonparametric method for analyzing spatial point data patterns is not related to specific parametric families of models, which only requires the intensity to be well-defined.

Our approach is not a direct replacement for current inference methods on few-variate spatial point processes (Jalilian et al., 2015). In contrast to the classical methodology, VAE requires a large number of training data. The highly multivariate data that are widely available in recommender systems and social networks can be ideal applications for our approach. In fact, it can be shown that our model is a generalization of a state-of-the-art VAE-based collaborative filtering model (Liang et al., 2018). Our model nonparametrically fits the underlying intensity function. Compared with the multinomial distribution used in Liang et al. (2018), this leads to not only a smoother intensity over space but also better predictions in terms of ranking-based losses. Compared to a univariate model, such as the trans-Gaussian Cox processes (Williams & Rasmussen, 2006), our multivariate model enhances the predictive ability on missing or unobserved areas, which is consistent with the results of heterogeneous multi-output Gaussian processes (Moreno-Muñoz et al., 2018).

The contributions of this paper are three-fold. We first build a novel multivariate spatial point process model and find a direct connection with the VAE-based collaborative filtering through detailed theoretical analysis. Secondly, this connection introduces amortized inference for an efficient multivariate point process estimation. Finally, point processes generalize the discrete distribution used in (Liang et al., 2018) and lead to better recommendations. We validate these benefits through extensive experiments for both synthetic and real-world multivariate data sets.

2 PRELIMINARIES

Spatial point process A *point process* (PP) is a random counting measure $N(x)$ on a complete separable metric space R (here we always assume that $R \subset \mathbb{R}^n$) that takes values on $\{0, 1, 2, ...\} \bigcup \{\infty\}$. While the major theory of point processes centers around the temporal dynamics, spatial point process models (Diggle et al., 1983) are established in forestry and seismology, focusing on the stationary and isotropic case. We focus on the (first-order) *intensity function* $\lambda(x)$, which is the expected rate of the accumulation of points around a particular spatial location x. We write

$$\lambda(x) = \lim_{|\Delta x| \downarrow 0} \frac{\mathbb{E}\left[N(\Delta x)\right]}{|\Delta x|}, \tag{1}$$

where Δx is a small ball in the metric space, e.g. the Euclidean space $\mathbb{R}^n$, with the centre x and measure $|\Delta x|$. The second-order intensity function is naturally defined as

$$\lambda_{(2)}(x, y) = \lim_{|\Delta x|, |\Delta y| \downarrow 0} \frac{\mathbb{E}\left[N(\Delta x)N(\Delta y)\right]}{|\Delta x||\Delta y|}, \tag{2}$$

measuring the chance of points co-occurring in both Δx and Δy. Normalizing this leads to the *pair-correlation function* $g(x, y) = \lambda_{(2)}(x, y)/\lambda(x)\lambda(y)$. $g(x, y) > 1$ indicates that points are more likely to attract each other and form clusters than the simple Poisson process where $g(x, y) = 1$.

Common models in SPP include the Poisson process with a non-stationary rate $\lambda(x)$, and the Cox process with a nonnegative-valued *intensity process* $\Lambda(x)$, which is also a stochastic process. Cox processes conditional on a realization of the intensity process $\Lambda(x) = \lambda(x)$ are Poisson processes with intensity $\lambda(x)$. To model the aggregated points patterns, Poisson cluster (Neyman-Scott) processes generate parent events from a Poisson process. Then each parent independently generates a random number of offsprings. The relative positions of these offsprings to the parent are distributed according to some p.d.f $K_\sigma(x)$ in space (Diggle et al., 1983). Many point process models, including most Cox processes, are in fact Poisson cluster processes. Repulsive SPPs, on the other hand, model that nearby points of the process tend to repel each other. Higher order intensities are often considered in this case, such as determinantal PPs.

Alternatively, if we are more interested in the realization intensity $\lambda(x)$ than the mechanical interpretation, the trans-Gaussian Cox process provides a tractable way to construct the Cox process using a nonlinear transformation on a Gaussian process $S(x)$. Popular choices for $\Lambda(x)$ include the log-Gaussian Cox process (LGCP) with $\exp(S(x))$ and the permanental process with $S(x)^2$. Recent works on Cox processes have been extensively focused on the cases that are modulated via the Gaussian random field, due to its capability in modeling the intensity and pair-correlations between subprocesses. In the next section, we develop a more explicit approach to model interactions for fast inference and the generalization ability for new subprocesses.

Inference for Point Processes   Inference methods for point processes are mainly based on the order statistics or likelihood function. The order statistics are often estimated nonparametrically, such as the kernel estimator (Diggle, 1985) of the intensity function. For the likelihood-based inference, we assume that one observes events $X = \{x_i\}_{i=1}^N$ of the underlying spatial point process over the area R. The log-likelihood for the inhomogeneous Poisson process over space R is

$$\log p(X|\Theta) = \sum_{i=1}^{N} \log(\lambda(x_i)) - \int_R \lambda(x)\, \mathrm{d}x\,. \tag{3}$$

The integration term is the log void probability and can be viewed as a normalization term for the likelihood. For Cox processes, the likelihood is the expectation over the Poisson likelihood. It is difficult to directly integrate over the distribution of Λ. Monte Carlo methods (Adams et al., 2009) are commonly used to approximate the expectation. To improve the scalability of the expensive sampling, many methods such as variational inference (Lloyd et al., 2015), Laplace approximation (Williams & Rasmussen, 2006) and reproducing kernel Hilbert spaces (Flaxman et al., 2017) are proposed.

Variational Autoencoder   As a stochastic variational inference algorithm, VAE (Kingma & Welling, 2014) is maximizing the evidence lower bound (ELBO) of the log-likelihood function

$$\log p(X|\Theta) \geq \mathbb{E}_{q_\phi(z|X)}[log(p_\theta(X|z)] - KL(q_\phi(z|X)|p(z)). \tag{4}$$

The hidden variables z have a simple multivariate Gaussian prior $p(z) = \mathcal{N}(z; 0, I)$. The true posterior, which is often intractable as in the Cox process, is approximated via a multivariate Gaussian $q_\phi(z|X) = \mathcal{N}(z; \mu_\phi(X), \sigma_\phi(X))$. The KL divergence term in the ELBO can be calculated analytically. VAE uses a multilayer perceptron (MLP) to learn the mean and variance of the approximated posterior directly from the data. The most related work here is a recent VAE-based model for collaborative filtering (VAE-CF) (Liang et al., 2018). They assume that each user is a multinomial distribution over items with the log-likelihood $\log p_\theta(X_u|z_u) = \sum_{i=1}^N X_{iu} \log \pi_i(z_u)$ for each user u. Here X_u is the observed data of user clicking items, $\pi_i(z_u)$ is the probability that user u clicks the item i and X_{iu} is an indicator function on whether the user u clicked the item i.

3   Multivariate Spatial Point Processes

Here we consider a multivariate case of the SPP, with U interdependent univariate point processes on the sample space R. The intensity function is measured in a similar way as the univariate case via $\lambda_u(x) = \lim_{|\Delta x|\downarrow 0} \left(\mathbb{E}\left[N_u(\Delta x)\right] / |\Delta x| \right)$, where $N_u(\Delta x)$ is the number of events within a set Δx for the subprocess u.

3.1   A nonparametric model

The observed data of multivariate SPP include the location of N_u events $X_u = \{x_i^u\}_{i=1}^{N_u}$ associated with each subprocess u. For each u, the observed event locations follow a Poisson process with spatial intensity $\lambda_u(x)$, which is a realization of the random intensity $\Lambda_u(x)$. Using the nonparameteric kernel estimator, the intensity of the subprocess u is estimated by

$$\lambda_u(x) = \sum_{i=1}^{N_u} K_\sigma(x - x_i^u). \tag{5}$$

Here $K_\sigma(x)$ is a kernel function and we usually adopt the radial basis function kernel (RBF) where $K_\sigma(x) = \exp(-\|x\|^2/2\sigma^2)$. We ignore the end-correction (Diggle, 1985) for now.

In real-world applications, however, one often encounters the missing data problem, where we cannot directly observe points in certain areas for some subprocesses. Instead, we seek to infer the hidden data from other fully observed subprocesses. Note that $N = \sum_{u=1}^U N_u$ is the total number of events. We introduce hidden variables Y_i^u for each event $x_i = 1, ..., N$ and subprocess $u = 1, ..., U$, where $Y_i^u = 1$ if the subprocess u includes event x_i and $Y_i^u = 0$ otherwise. $\mathbb{E}Y_i^u = p_i^u$ is the probability that event x_i is from the subprocess u. Then the intensity process for our multivariate

SPP model is

$$\Lambda_u(x) = \sum_{i=1}^{N} Y_i^u K_\sigma(x - x_i), \tag{6}$$

for each subprocess u. This model generalizes the kernel density-based intensity to the missing data case. Similarly to the original method, it can be applied to estimate the intensity for both cluster processes such as Cox processes and repulsive ones like determinantal PPs. In order to incorporate prior information and model the data uncertainty, we adopt a variational inference approach for the hidden variables.

3.2 VARIATIONAL INFERENCE

A major drawback of current inference methods for SPP is the introduction of a large number of parameters in the highly multivariate case. For our model, we use an amortized inference approach - VAE (Kingma & Welling, 2014) to avoid the computational complexity of directly estimating the posterior for each subprocess u.

The generative process of our model can be described as follow: For each subprocess u, it has a K-dimensional hidden variable z_u with a multivariate normal prior $z_u \sim \mathcal{N}(0, I_K)$. Here we use a low-dimensional representation and then a nonlinear mapping $f_\theta(z_u) = \{p_i^u\}_{i=1}^{N}$ transforms z_u so that it has the same dimension as the number of events N. Finally the spatial points of the subprocess u are sampled according to the intensity $\lambda(x) = \sum_{i=1}^{N} p_i^u K_\sigma(x - x_i)$. We approximate the intractable posterior distribution of z, $q(z|X)$ with a multivariate Gaussian $\mathcal{N}(\mu_\phi(X), \sigma_\phi(X))$. As in Liang et al. (2018), we use MLPs to learn the nonlinear function $f_\theta(z)$ with parameters θ and the mean and variance with parameters ϕ. The variational bound of our multivariate Cox process model is then

$$\log p(X_u|\Theta) \geq \mathbb{E}_{q_\phi(z_u|X_u)}[log(p_\theta(X_u|z_u)] - KL(q_\phi(z_u|X_u)|p(z_u)) = \mathbf{L}. \tag{7}$$

The first term in $\mathbf{L}$ is essentially a complete likelihood function. For each subprocess u, it has the following (expected) intensity function

$$\mathbb{E}_{q_\phi(z_u|X_u)}\Lambda_u(x) = \sum_{i=1}^{N_u} p_i^u K_\sigma(x - x_i^u) \tag{8}$$

and a Poisson process log-likelihood function from (8) and (3)

$$\mathbb{E}_{q_\phi(z_u|X_u)} \log p_\theta(X_u|z_u) = \sum_{i=1}^{N_u} \log(\sum_{i=1}^{N_u} p_i^u K_\sigma(x - x_i^u)) - \int_R \sum_{i=1}^{N_u} p_i^u K_\sigma(x - x_i^u)dx. \tag{9}$$

For applications without explicit spatial information, we embed each event into a latent space as a vector. First, we obtain a similarity graph for all events. Then the embedding x_i of i_{th} event in this graph is obtained via graph neural networks (GNNs) such as GraphSAGE (Hamilton et al., 2017). See Figure 1 for an illustration of our framework.

3.3 ALTERNATIVE MODEL

Recall that the hidden variables Y_i^u describe whether the event x_i is from the subprocess u. By definition, we have $\sum_{u=1}^{U} Y_i^u = 1$ and $\sum_{u=1}^{U} p_i^u = 1$ for any i. During the training process, it is difficult to normalize the probability p_i^u over all subprocesses (have to use the full data). Moreover, this constraint leads to $g_{uv} < 1$ for $u \neq v$, implying mutual-inhibition behaviors between subprocesses. Instead, we consider an alternative model where p_i^u is the probability that the subprocess u generates an event x_i i.e. $\sum_{i=1}^{N} p_i^u = 1$ for each u. During the training, the total number of events N_u is not viewed as a hidden variable for each subprocess. Thus the alternative model essentially normalizes λ_u by a constant. With the reparameterization trick in Kingma & Welling (2014), we sample the log-likelihood function using all events within a mini user batch and compute the gradient. This approach incorporates all information about the user so that negative sampling is not needed. See Algorithm 1 for our training procedure. For the model prediction, the normalized intensity of a new subprocess can be efficiently calculated in $O(N)$ using the approximated posterior $q_\phi(z|X_{new})$
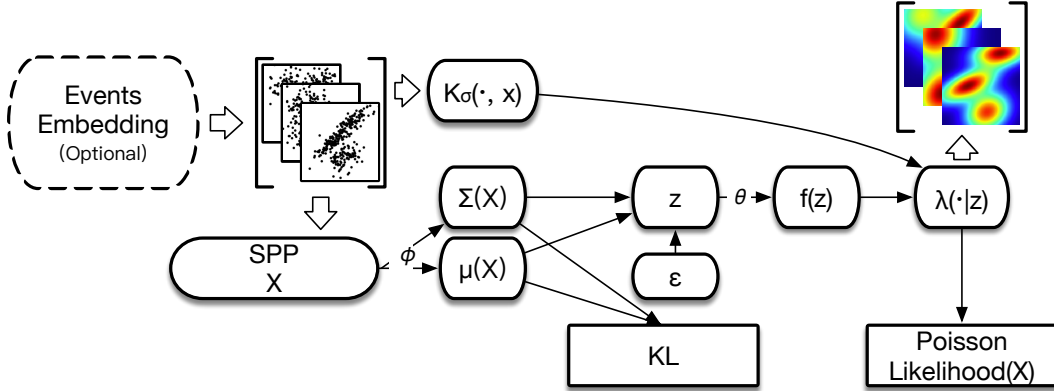
Figure 1: Visual illustration of our spatial point process model via VAE during the training.

and nonlinear function $f_\theta(z)$ with parameters θ, ϕ inferred from data. We can further reduce the computational challenge (Liang et al., 2018) for large N due to $f_\theta(z)$ by discretizing the space.

Now we show the equivalence of our multivariate model and the alternative one. There are two probabilities to consider. The first one is the conditional probability of observed events X_u in the subprocess u with an intensity function $\lambda_u(x)$, given that there are N_u events within the metric space R. The second one is the probability of sample X_u of size N_u from the normalized density $h_u(x) = \lambda_u(x)/\int_R \lambda_u(s)ds$. For general SPPs data, we have

Theorem 1. *A spatial point process on a measurable set $R \subset \mathbb{R}^n$ with an intensity function $\lambda_u(x)$ is equivalent to N_u i.i.d samples within R with p.d.f $h_u(x) = \lambda_u(x)/\int_R \lambda_u(s)ds$, given we know $N_u = \int \lambda_u(s)ds$, which is the number of points within R for the point process model.*

Proof. See Section B in Appendix. □

According to this theorem (see supplementary material), we can replace the log-likelihood function (9) in the ELBO with

$$\mathbb{E}_{q_\phi(z_u|X_u)} \log p_\theta(X_u|z_u) = \sum_{i=1}^{N_u} \log(h_u(x_i^u)) + C. \qquad (10)$$

Here C is related to the log-likelihood on the number of events N_u, which is a constant because $\int_R \lambda_u(s)ds = N_u$ is observed. One drawback of this approach is that, for the prediction of actual missing data, we cannot infer the number of missing points. Instead, our VAE-based model generates the normalized intensity predicting the possible locations for the missing events. We use the alternative definition of p_i^u from now on. This result also shows that VAE-CF is a special case of this multivariate spatial point process model over a discrete space X of events. This is because that VAE-CF uses a delta function as the kernel and then $h_u(x_i) = \lambda_u(x_i)/\int_X \lambda_u(s)ds = p_i^u$. In the general case on a continuous space, we can replace the δ function with other kernels such as RBF, resulting in $h_u(x) = \sum_{i=1}^N p_i^u \exp(\|x - x_i\|^2/2\sigma^2)$.

One benefit of this alternative model is its resulted consistency. The nonparametric kernel estimation for the point process intensity is unbiased. To see this, for any measurable set R, we take the expectation of the estimated intensity $\lambda(x)$ over the Poisson point process distribution

$$\mathbb{E}\int_R \lambda(x)dx = \int_R \mathbb{E}\sum_{i=1}^N K_\sigma(x - x_i)dx = \int_R \int_R K_\sigma(x - y)\rho(y)dydx = \int_R \rho(y)dy, \qquad (11)$$

where $\rho(y)$ is the true intensity function. Then $\mathbb{E}\lambda(x) = \rho(x)$ under mild conditions, e.g., a spatially continuous assumption on ρ. But it is inconsistent due to the non-vanishing variance without normalization. For our alternative model, the normalized intensity function $h_u(x)$ is still unbiased.

Algorithm 1: Training VAE SPP with stochastic gradient descent.

Input: Traning subprocesses $u \in \mathbf{U_T}$ with their point locations X_u
Result: Parameters θ and ϕ
Initialize θ and ϕ randomly;
while *not converged* **do**
    Sample a subprocesses batch $\mathbf{U_b}$ from $\mathbf{U_T}$ and their points $X_b = \bigcup_{u \in \mathbf{U_b}} X_u$;
    forall $u \in \mathbf{U_b}$ **do**
        Sample $z_u \sim \mathcal{N}(\mu_\phi(X_u), \sigma_\phi(X_u))$ with reparameterization trick;
        Compute $f_\theta(z_u) = \{p_i^u\}_{x_i \in X_b}$;
        forall $x \in X_u$ **do**
            Compute sampled normalized intensity $h_u(x) \approx \sum_{x_i \in X_b} p_i^u K_\sigma(x - x_i)$;
        end
        Compute noisy gradients of the ELBO $\mathbf{L}$ w.r.t θ and ϕ
    end
    Average noisy gradients over batch;
    Update θ and ϕ with the Adam optimizer (Kingma & Ba, 2015);
end

And according to the standard theory of the multivariate kernel density estimation (KDE), the consistency of $h_u(x)$ is also guaranteed. Another benefit of using this alternative form can be seen from the cross pair-correlation function. For the alternative model, we remove the undesirable restriction of negative correlations between all users ($g_{uv} < 1$ for $u \neq v$) and can incorporate more diverse relationships between users. To see this, we first consider the *auto* and *cross pair-correlation function* $g_{uv} = \mathbb{E}\Lambda_u \Lambda_v / \mathbb{E}\Lambda_u \mathbb{E}\Lambda_v$. For our original model, it is straightforward to prove that $g_{uu} > 1$ and $g_{uv} < 1, u \neq v$ (see supplementary material). The auto pair-correlation functions show that our model is more aggregate than the simple Poisson process.

4 EXPERIMENTS

We compare our model (with the RBF kernel, VAE-SPP) with both VAE-CF (Liang et al., 2018) and univariate spatial point process models using a standard KDE (Diggle, 1985) or TGCP (Williams & Rasmussen, 2006) as intensity functions. We adopt the experiment setting in VAE-CF. We split the data into training, validation and testing sets. For the multivariate model, the training data is used to learn the parameters θ, ϕ. For KDE and TGCP models, we omit the training data because different subprocesses are assumed to be independent and also because of the computational complexity of fitting a highly multivariate TGCP. We assume that only 80% of the events in the validation and test sets are observed. The remaining 20% are viewed as missing data to be inferred by different models. Hyperparameters are selected on the validation data as in Liang et al. (2018). Finally, we compare the prediction performance of different models on the missing data given the partially-observed events. We use standard ranking losses such as normalized discounted cumulative gain at k (NDCG@k) and recall at k (Recall@k) defined in Liang et al. (2018).

4.1 MULTIVARIATE SPP ON SPATIAL DATA

Synthetic data sets We simulate two different data sets using multiexponential and multisine models. For the multiexponential data set, we simulate 5,000 Poisson processes with $\lambda_k(x) = a_k e^{-b_k x}, k = 1, ..., 5000, x \in [0, 30]$ as training data. Here a_k and b_k are uniformly sampled between $[5, 10]$ and $[0.1, 0.2]$ separately. 500 validation and 500 test subprocesses are generated in the same way with parameters sampled from a_k and b_k. The multisine data set is generated via replacing the intensity function with $\lambda_k(x) = \max(a_k * \sin(b_k x), 5)$ and sampling a_k and b_k uniformly between $[5, 10]$ and $[1, 2]$ separately. Each realization of the spatial point process is discretized using a uniform grid over x with grid spacing 0.01.

Location-based Social Network. We consider the Gowalla data set (Cho et al., 2011) in New York City (NYC) and California (CA). We use a bounding box of -124.4096, 32.5343, -114.1308,

Table 1: Testing results on the simulation data sets. Both the mean and variance are percentages (same below).

Name	Multiexp			Multisine		
	NDCG@100	Recall@50	Recall@100	NDCG@100	Recall@50	Recall@100
VAE-CF	6.78(0.28)	7.25(0.40)	14.5(0.52)	3.30(0.15)	2.49(0.13)	4.64(0.18)
VAE-SPP	**7.11**(0.31)	**7.34**(0.40)	**14.9**(0.54)	3.53(0.15)	**2.58**(0.13)	**4.90**(0.18)
KDE	5.27(0.15)	5.85(0.12)	11.8(0.17)	3.23(0.15)	2.29(0.12)	4.55(0.27)
TCGP	3.11(0.14)	3.32(0.11)	6.44(0.11)	**3.77**(0.14)	1.88(0.11)	3.92(0.17)

42.0095 for CA and -74.0479, 40.6829, -73.9067, 40.8820 for NYC (both from flickr[1]). Each user with at least 20 events (check-ins) is viewed as a subprocess. There are 673,183 events and 6,728 users for Gowalla-CA. We randomly select 500 users as the validation set and 500 users as the testing set. We use the remaining users for training. For Gowalla NYC, there are 86,703 events from 1,171 users. We set the size of both validation and testing sets to 100. For the spatial tessellation, we use uniform grids (32×32 for NYC and 64×64 for CA). Both our model and VAE-CF can work without grids. We further compare the performance of our model with VAE-CF by viewing each location as an item.

Table 2: Testing results on the Gowalla data sets with uniform grids.

Name	CA			NYC		
	NDCG@100	Recall@50	Recall@100	NDCG@100	Recall@50	Recall@100
VAE-CF	41.8(1.5)	64.8(2.0)	70.0(2.0)	43.6(2.3)	73.9(2.9)	**86.2**(2.2)
VAE-SPP	**42.3**(1.5)	**65.2**(2.0)	**70.2**(1.9)	**44.8**(2.4)	**74.5**(2.9)	**86.2**(2.2)
KDE	34.5(1.5)	59.2(2.0)	64.0(2.0)	41.2(1.5)	69.9(2.0)	83.6(2.0)
TCGP	31.8(1.3)	56.5(2.0)	60.9(2.0)	37.3(2.3)	59.9(3.3)	75.9(2.8)

Table 3: Testing results on the Gowalla data sets without discretization.

Name	CA			NYC		
	NDCG@100	Recall@20	Recall@100	NDCG@100	Recall@20	Recall@100
VAE-CF	21.3(0.77)	16.6(0.74)	32.8(0.97)	16.0(1.7)	13.2(1.7)	26.3(2.4)
VAE-SPP	**21.6**(0.77)	**17.0**(0.80)	**33.5**(0.76)	**16.1**(1.7)	**13.7**(1.8)	**27.1**(2.5)

In Table 1, we summarize the performance of both multivariate and univariate models on the simulation data sets. It is clear that the multivariate models outperform the univariate ones. Moreover, testing on multivariate models takes less time because it only evaluates the posterior probability and intensity function. This illustrates the power of multivariate models using amortized inference. Within the multivariate models, our continuous model further improves upon the discrete VAE-CF. This is due to the fact that these simulation intensities are continuous over R. For real-world applications, the results on the location-based social network prediction and recommendation with and without grids are presented in Table 2 and 3. We observe the same pattern in both NYC and CA. We stop using univariate models from now on due to their inferior performances, especially for collaborative filtering applications. Moreover, our model improves discrete VAE-CF regardless of the choice of spatial grids. For visualization purposes, in Figure 2, we plot a user's check-in locations in Gowalla-NYC and intensities estimated via different methods. Comparing with VAE-CF, our model generates a continuous intensity. The univariate models overfit the training data and lead to inferior predictions of the missing data.

4.2 MULTIVARIATE SPP WITH A LATENT SPACE

MovieLens data sets (ML-100K and ML-1M) include the movie (item) rating by users and we binarize the rating with a threshold of 4. In the spatial point process setting, we view each user as a subprocess over the latent space of item embeddings. Here the item embedding is generated via a GNN. This framework is a natural generalization of the multimodal distribution over items.

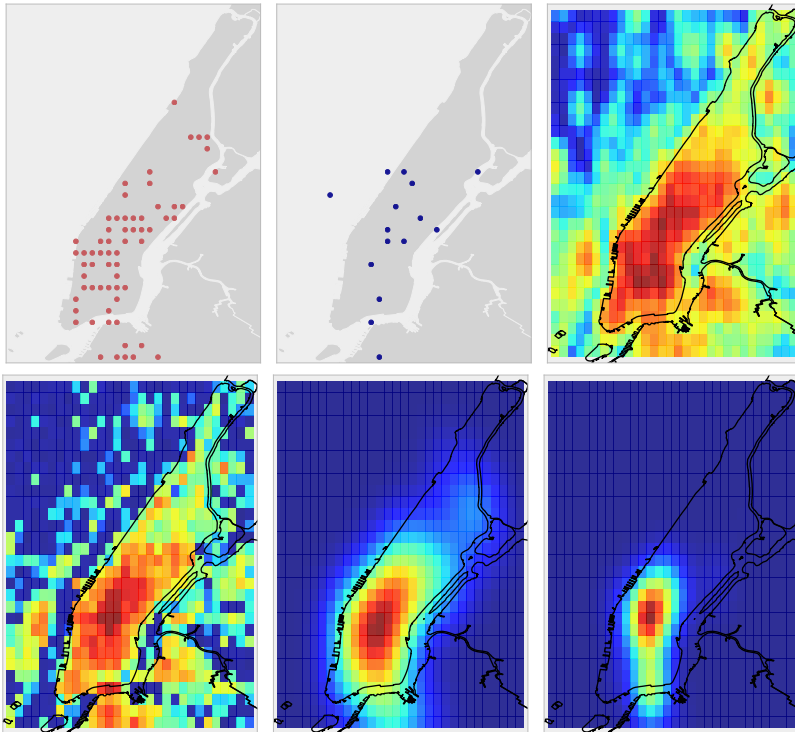[1]https://www.flickr.com/places/info/

Figure 2: Estimated density functions for a Gowalla user in NYC (log scale). The first row from left to right: observed check-in locations (in red), held-out check-in locations (in blue, as missing data) and the estimated intensity from VAE-SPP. The second row from left to right: the estimated intensity (or density) from VAE-CF, KDE and TGCP.

The item-item graph is constructed based on item-item similarities. We use the Jaccard distance to measure the similarities between items, which are further viewed as the sampling probabilities for GNN. Currently, we only consider 1-hop connections. Both GNN and VAE are trained jointly, which according to our experiments leads to better performance compared to separate training. For movie recommendation tasks, we compare the discrete VAE-CF to our joint model with GNN. The results in Table 4 show again the improvement of our model over the baseline.

Table 4: Testing results on the MovieLens data sets.

	ML100K			ML1M		
Name	NDCG@100	Recall@20	Recall@100	NDCG@100	Recall@20	Recall@100
VAE-CF	40.8(2.8)	**32.3**(2.8)	57.6(3.3)	41.6(0.76)	33.1(0.81)	56.8(0.88)
VAE-SPP	**41.5**(2.9)	31.3(2.7)	**59.0**(3.5)	**42.3**(0.77)	**33.9**(0.82)	**57.6**(0.88)

5 CONCLUSION

In this paper, we introduce a novel spatial point process model for efficient inference on the highly multivariate case. Through amortized inference, our model makes it possible to investigate correlations between a myriad of point patterns based on a large number of training data, and the theoretical analysis builds the connection between our model and VAE-CF. There are many promising directions of future works including the extension for spatiotemporal PPs (Mohler et al., 2011) and using features as covariances. Another interesting application is to handle the cold-start problem of the new items using our latent space approach, due to the inductive ability of GNN (Hamilton et al., 2017) to generate embeddings.

REFERENCES

Ryan Prescott Adams, Iain Murray, and David JC MacKay. Tractable nonparametric bayesian inference in poisson processes with gaussian process intensities. In *Proceedings of the 26th Annual International Conference on Machine Learning*, pp. 9–16. ACM, 2009.

Eunjoon Cho, Seth A Myers, and Jure Leskovec. Friendship and mobility: user movement in location-based social networks. In *Proceedings of the 17th ACM SIGKDD international conference on Knowledge discovery and data mining*, pp. 1082–1090. ACM, 2011.

Achmad Choiruddin, Francisco Cuevas-Pacheco, Jean-François Coeurjolly, and Rasmus Waagepetersen. Regularized estimation for highly multivariate log gaussian cox processes. *arXiv preprint arXiv:1905.01455*, 2019.

Peter Diggle. A kernel method for smoothing point process data. *Journal of the Royal Statistical Society: Series C (Applied Statistics)*, 34(2):138–147, 1985.

Peter J Diggle et al. *Statistical analysis of spatial point patterns.* Academic press, 1983.

Seth Flaxman, Yee Whye Teh, Dino Sejdinovic, et al. Poisson intensity estimation with reproducing kernels. *Electronic Journal of Statistics*, 11(2):5081–5104, 2017.

Samuel Gershman and Noah Goodman. Amortized inference in probabilistic reasoning. In *Proceedings of the annual meeting of the cognitive science society*, volume 36, 2014.

Will Hamilton, Zhitao Ying, and Jure Leskovec. Inductive representation learning on large graphs. In *Advances in Neural Information Processing Systems*, pp. 1024–1034, 2017.

Xiangnan He, Lizi Liao, Hanwang Zhang, Liqiang Nie, Xia Hu, and Tat-Seng Chua. Neural collaborative filtering. In *Proceedings of the 26th International Conference on World Wide Web*, pp. 173–182. International World Wide Web Conferences Steering Committee, 2017.

Abdollah Jalilian, Yongtao Guan, Jorge Mateu, and Rasmus Waagepetersen. Multivariate product-shot-noise cox point process models. *Biometrics*, 71(4):1022–1033, 2015.

Diederik P Kingma and Jimmy Ba. Adam: A method for stochastic optimization. *ICLR*, 2015.

Diederik P Kingma and Max Welling. Auto-encoding variational bayes. *ICLR*, 2014.

Wenzhao Lian, Ricardo Henao, Vinayak Rao, Joseph Lucas, and Lawrence Carin. A multitask point process predictive model. In *International Conference on Machine Learning*, pp. 2030–2038, 2015.

Dawen Liang, Rahul G Krishnan, Matthew D Hoffman, and Tony Jebara. Variational autoencoders for collaborative filtering. In *Proceedings of the 2018 World Wide Web Conference on World Wide Web*, pp. 689–698. International World Wide Web Conferences Steering Committee, 2018.

Chris Lloyd, Tom Gunter, Michael Osborne, and Stephen Roberts. Variational inference for gaussian process modulated poisson processes. In *International Conference on Machine Learning*, pp. 1814–1822, 2015.

George O Mohler, Martin B Short, P Jeffrey Brantingham, Frederic Paik Schoenberg, and George E Tita. Self-exciting point process modeling of crime. *Journal of the American Statistical Association*, 106(493):100–108, 2011.

Pablo Moreno-Muñoz, Antonio Artés, and Mauricio Álvarez. Heterogeneous multi-output gaussian process prediction. In *Advances in Neural Information Processing Systems*, pp. 6711–6720, 2018.

Benjamin Taylor, Tilman Davies, Barry Rowlingson, and Peter Diggle. Bayesian inference and data augmentation schemes for spatial, spatiotemporal and multivariate log-gaussian cox processes in r. *Journal of Statistical Software*, 63:1–48, 2015.

Christopher KI Williams and Carl Edward Rasmussen. *Gaussian processes for machine learning*, volume 2. MIT Press Cambridge, MA, 2006.

Jiancang Zhuang, Yosihiko Ogata, and David Vere-Jones. Stochastic declustering of space-time earthquake occurrences. *Journal of the American Statistical Association*, 97(458):369–380, 2002.

A   TABLE OF NOTATIONS

Table 5: Notations.

Notation	Definition or Descriptions
$N(x)$	counting measure on a metric space R
N_u	the number of events of subprocess u
$\lambda_u(x)$	intensity function of a subprocess u
$\Lambda_u(x)$	intensity process of a subprocess u
$K_\sigma(x)$	kernel function
U	# of subprocesses on the space
$\mathbf{U}_b$	subprocesses in a batch
X	events set
X_u	observed events of subprocess u
X_b	all the observed events in a batch of subprocesses
x_i	embedding/location of the i_{th} event
Y_i^u	hidden variables indicate whether the subprocess u includes the i_{th} event
z_u	K-dimensional hidden variable represents subprocess u
p_i^u	probability of the i_{th} event occurs in subprocess u
ϕ, θ	parameters of encoder(μ_ϕ, σ_ϕ) and decoder(f_θ)
$g_{uv} = \mathbb{E}\Lambda_u\Lambda_v/\mathbb{E}\Lambda_u\mathbb{E}\Lambda_v$	auto and cross pair-correlation function
$h_u(x)$	normalized density

B   PROOF OF THEOREM 1

Proof. We define our model as a point process on R with the intensity function $\lambda_u(x)$.

The alternative model is N_u i.i.d samples within R with p.d.f $h_u(x)$, given that we know $N_u = \int \lambda_u(s)ds$ is the number of points within the point process model.

1) Our model has the following probability generating functional

$$G(v) = \exp(-\int_{\mathbf{R}^d} [1 - v(x)] \Lambda(\mathrm{d}x)) \tag{12}$$

2) Given N_u,

$$p(x_1, ..., x_{N_u}|N_u) = \prod_{i=1}^{N_u} h_u(x_i) \tag{13}$$

3) Our alternative model (a counting r.v. $N(x)$ with locations according to $h_u(x)$) has the following characteristic functional

$$G_c(v) = \sum_{n=0}^{\infty} p(N(R) = n)\mathbb{E}[\exp(\int_R \log(v(s))N(ds))|N(R) = n] \tag{14}$$

Using 2), we can evaluate this conditional probability

$$\mathbb{E}[\exp(\int_R \log(v(s))N(ds))|N(R) = n] = (\frac{\int_R \lambda_u(s)v(s)ds}{\lambda_u(s)ds})^n \qquad (15)$$

Using 2) again and because the point process observation probability is

$$p(\omega) = p(N(R) = N_u)p(x_1, ..., x_{N_u}|N_u) = \frac{1}{n!}[\prod_{i=1}^{n} \lambda_u(x_i)] \exp(-\int_R \lambda(x)dx), \qquad (16)$$

we have

$$G_c(v) = \exp(-\int_R \lambda(x)dx)(1 + \sum_{n=1}^{\infty} \frac{1}{n!}(\int_R \lambda(s)v(s)ds)^n) = \exp(\int_R \lambda(s)(v(s) - 1)ds). \qquad (17)$$

The theorem follows from $G_c(v) = G(v)$ as the probability generating functional completely determines the probability structure of the point process. $\qquad \square$

We show that (10) holds in the main paper.

Corollary 1.1.

$$\mathbb{E}_{q_\phi(z_u|X_u)} \log p(X_u|z_u) = \sum_{i=1}^{N_u} \log(h_u(x_i^u)) + C. \qquad (18)$$

Proof. Define $\lambda_u(x) = \mathbb{E}_{q_\phi(z_u|X_u)}\Lambda_u(x)$.

$$\mathbb{E}_{q_\phi(z_u|X_u)} \log p(X_u|z_u) = \log \left(p(N(R) = N_u)p(x_1^u, ..., x_{N_u}^u|N_u) \right) \qquad (19)$$

$$= \sum_{i=1}^{N_u} \log(h_u(x_i^u)) + \log(p(N(R) = N_u)) \qquad (20)$$

$$\log(p(N(R) = N_u)) = n \log(\int_R \lambda(x)dx) - \log(n!) - \int_R \lambda(x)dx \qquad (21)$$

is only a function of N_u. $\qquad \square$

C AUTO AND CROSS PAIR-CORRELATION FUNCTIONS

We show that $g_{u,v}(x, y) > 1$ for $u = v$ and $g_{u,v}(x, y) < 1$ for $u \neq v$ for our orginal model.

$$g_{u,v}(x, y) = \frac{\mathbb{E}\Lambda_u(x)\Lambda_v(x)}{\mathbb{E}\Lambda_u(x)\mathbb{E}\Lambda_v(x)} \qquad (22)$$

We have

$$\mathbb{E}\Lambda_u(x)\Lambda_v(x) = \mathbb{E}(\sum_{i=1}^{N} Y_i^u K_h(x - x_i))(\sum_{j=1}^{N} Y_j^v K_h(y - x_j)) \qquad (23)$$

$$= \sum_{i=1}^{N} \sum_{j=1}^{N} \mathbb{E}Y_i^u Y_j^v K_h(x - x_i)K_h(y - x_j). \qquad (24)$$

Similarly,

$$\mathbb{E}\Lambda_u(x)\mathbb{E}\Lambda_v(x) = (\mathbb{E}\sum_{i=1}^{N} Y_i^u K_h(x - x_i))(\mathbb{E}\sum_{j=1}^{N} Y_j^v K_h(y - x_j)) \qquad (25)$$

$$= \sum_{i=1}^{N} \sum_{j=1}^{N} p_i^u p_j^v K_h(x - x_i)K_h(y - x_j). \qquad (26)$$

Note that $\sum_{u=1}^{U} Y_i^u = 1$ and $\sum_{u=1}^{U} p_i^u = 1$. When $i \neq j$, we have $\mathbb{E}Y_i^u Y_j^v = p_i^u p_j^v$ for any u, v. When $i = j$, $\mathbb{E}Y_i^u Y_i^u = p_i^u > (p_i^u)^2$ for $u = v$ and $\mathbb{E}Y_i^u Y_i^v = 0 < p_i^u p_i^v$. Then it is easy to see $g_{u,v}(x, y) > 1$ for $u = v$ and $g_{u,v}(x, y) < 1$ for $u \neq v$.

D   ADDITIONAL EXPERIMENTS

On the training of VAE and GNN, we tried different settings and choose to train them jointly.

Table 6: Testing results on MovieLens-100K. These methods share the same VAE network and trained with 100 epochs. The test data is evaluating the model with the best performance during the validation. Separate means that GNN is trained separately with VAE-SPP.

	NDCG@100	Recall@20	Recall@100
VAE-CF	0.4088	0.3232	0.5763
VAE-SPP	0.4150	0.3134	0.5899
VAE-SPP-Separate	0.4143	0.3115	0.5882

We also did experiments on the MLPs for VAE. For Movie Lens 1M, the larger network in VAE-CF leads to a 40.3 NDCG@100 for VAE-CF and 41.9 for VAE-SPP. As a result, we use the smaller one instead.